Electronic Supplementary Material (ESI) for Journal of Materials Chemistry A.
This journal is © The Royal Society of Chemistry 2019

Supporting Information

Unravelling the Impact of Electrolyte Nature on Sn_4P_3/C Negative Electrodes for Na-ion Batteries

Juan Luis Gómez-Cámer[1,], Begoña Acebedo[1], Nagore Ortiz-Vitoriano[1,2], I. Monterrubio[1], Montserrat Galcerán[1], Teófilo Rojo[1,3,*]*

1 CIC EnergiGUNE, Albert Einstein 48, Technology Park of Álava, 01510 Miñano (Álava), Basque Country, Spain

2 IKERBASQUE, Basque Foundation for Science, 48013 Bilbao, Spain

3 Inorganic Chemistry Department, University of the Basque Country UPV/EHU, P.O. Box 644, 48080, Bilbao, Spain

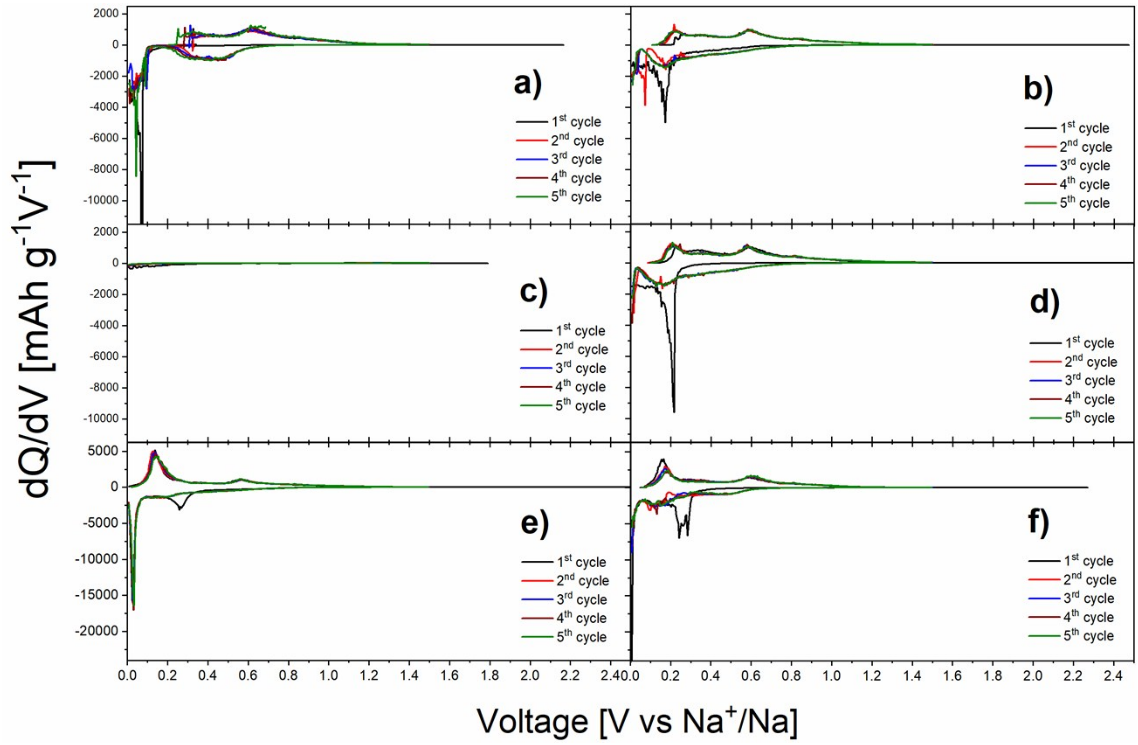

Figure S1. Derivative curves of the five initial charge/discharge cycles of Sn_4P_3/C electrodes cycled in a) $NaClO_4$/EC:PC, b) $NaClO_4$/EC:PC:FEC, c) $NaPF_6$/EC:PC, d) $NaPF_6$/EC:PC:FEC, e) $NaPF_6$/DEGDME and f) $NaPF_6$/DEGDME:FEC electrolyte.

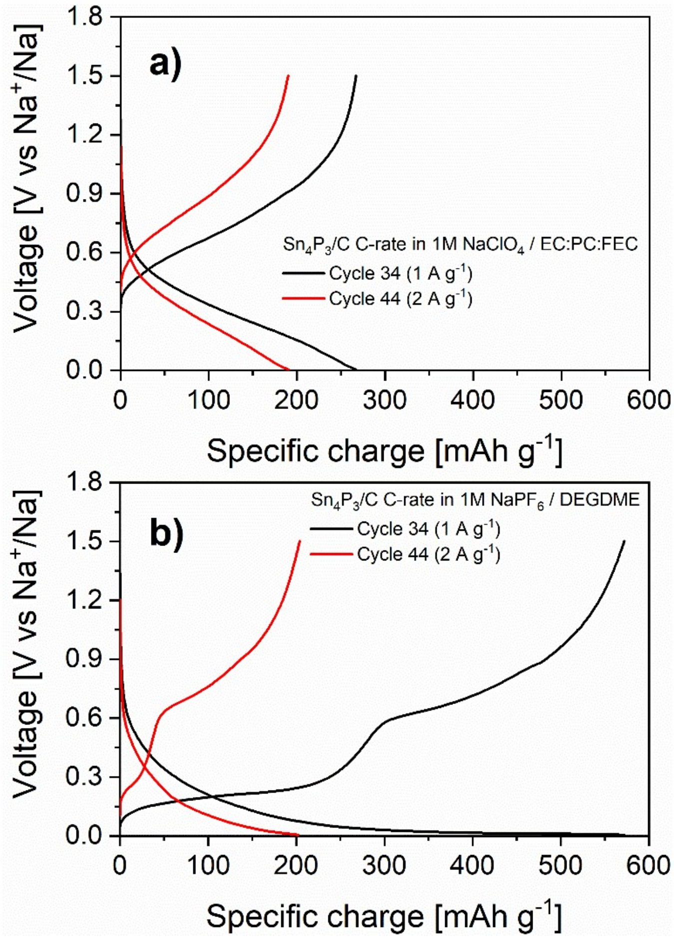

Figure S2. Galvanostatic curves of the 34th and 44th cycle at 1 A g^{-1} and 2 A g^{-1} of the Sn_4P_3/C electrodes in (a) 1M $NaClO_4$/EC:PC:FEC and (b) 1M $NaPF_6$/DEGDME electrolytes.

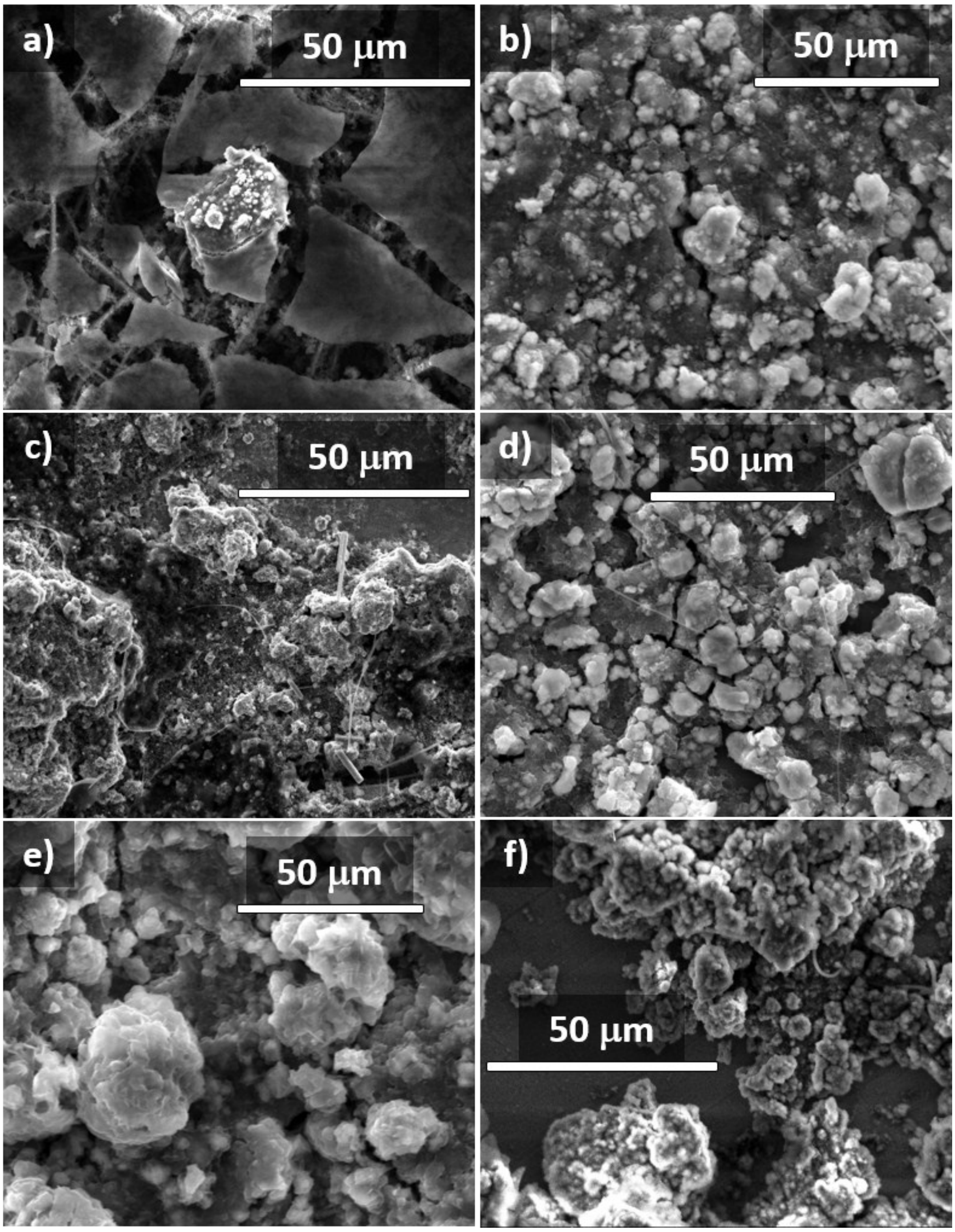

Figure S3. SEM images of Sn_4P_3/C electrodes after 100 charge/discharge cycles in a) $NaClO_4$/EC:PC, b) $NaClO_4$/EC:PC:FEC, c) $NaPF_6$/EC:PC, d) $NaPF_6$/EC:PC:FEC, e) $NaPF_6$/DEGDME and f) $NaPF_6$/DEGDME:FEC electrolytes.

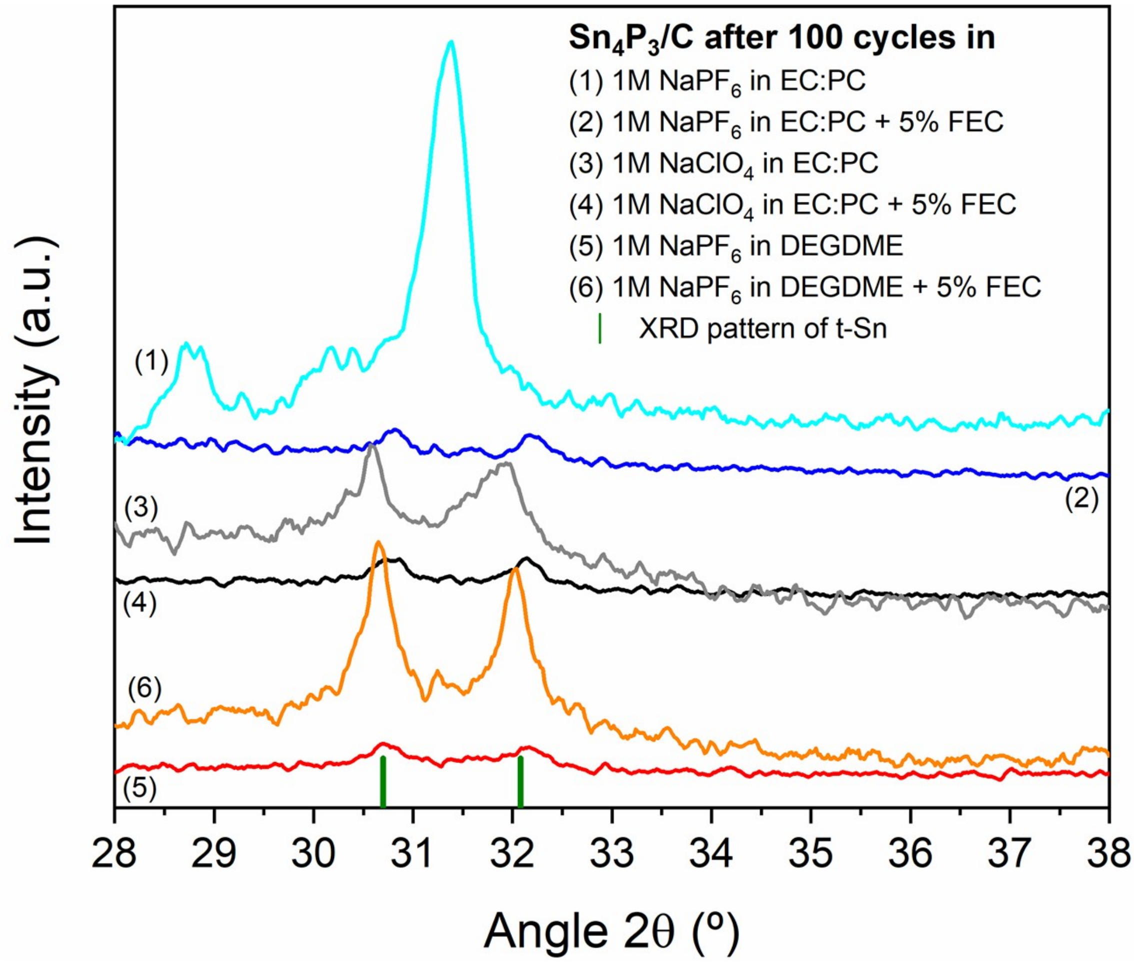

Figure S4. X-ray diffractograms of the Sn_4P_3/C electrodes after 100 charge/discharge cycles in the different electrolytes. The green bars indicate the position of the most intense peaks of the t-Sn reference.

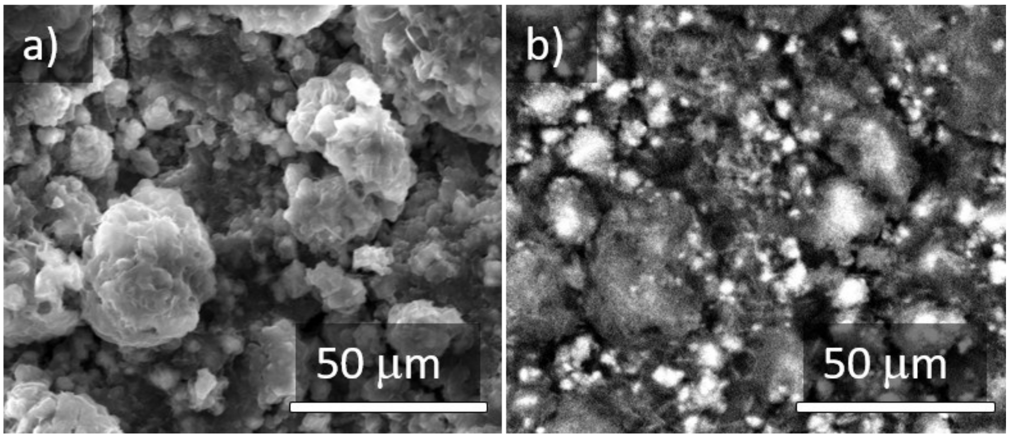

Figure S5. SEM (a) and BSE (b) images of Sn_4P_3/C electrode after 100 cycles in $NaPF_6$/DEGDME electrolyte. The heavier elements are shown as brighter spots in the BSE images.

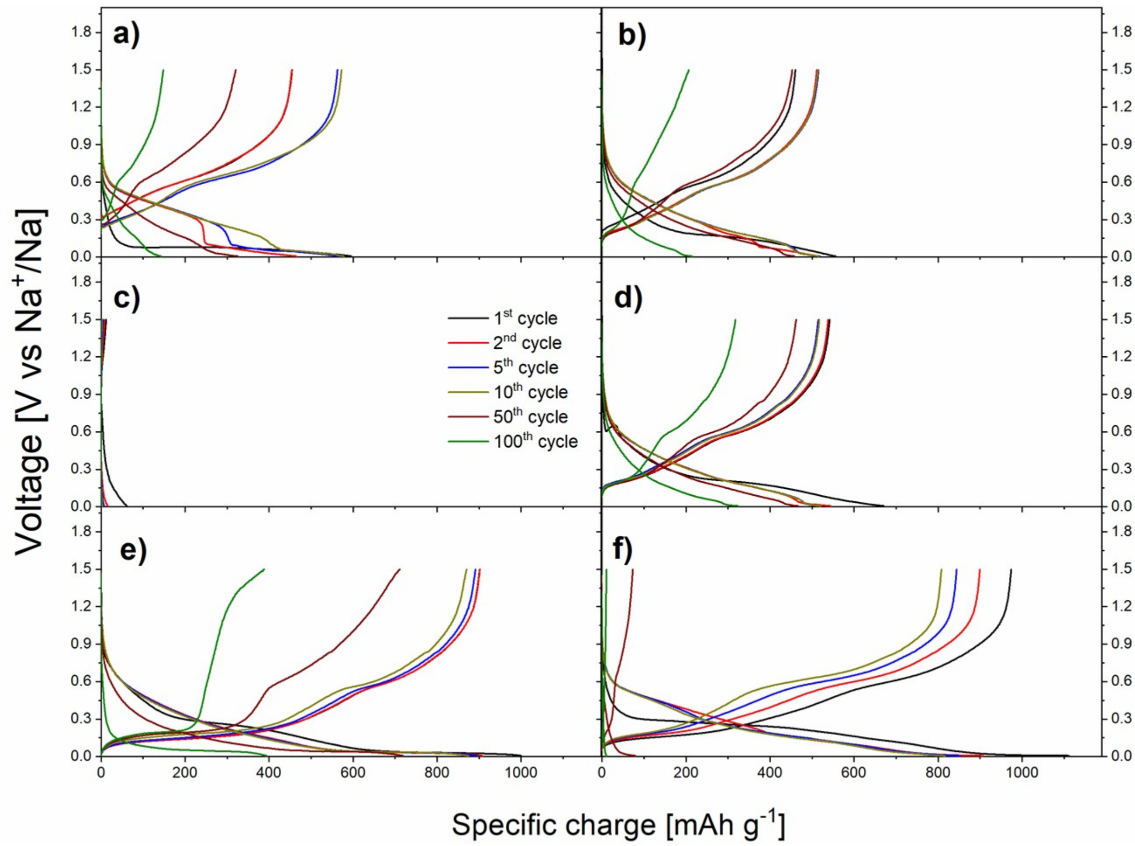

Figure S6. Galvanostatic curves of the 1st, 2nd, 5th, 10th, 50th and 100th charge/discharge cycles of Sn_4P_3/C electrodes cycled in a) $NaClO_4$/EC:PC, b) $NaClO_4$/EC:PC:FEC, c) $NaPF_6$/EC:PC, d) $NaPF_6$/EC:PC:FEC, e) $NaPF_6$/DEGDME and f) $NaPF_6$/DEGDME:FEC electrolyte.

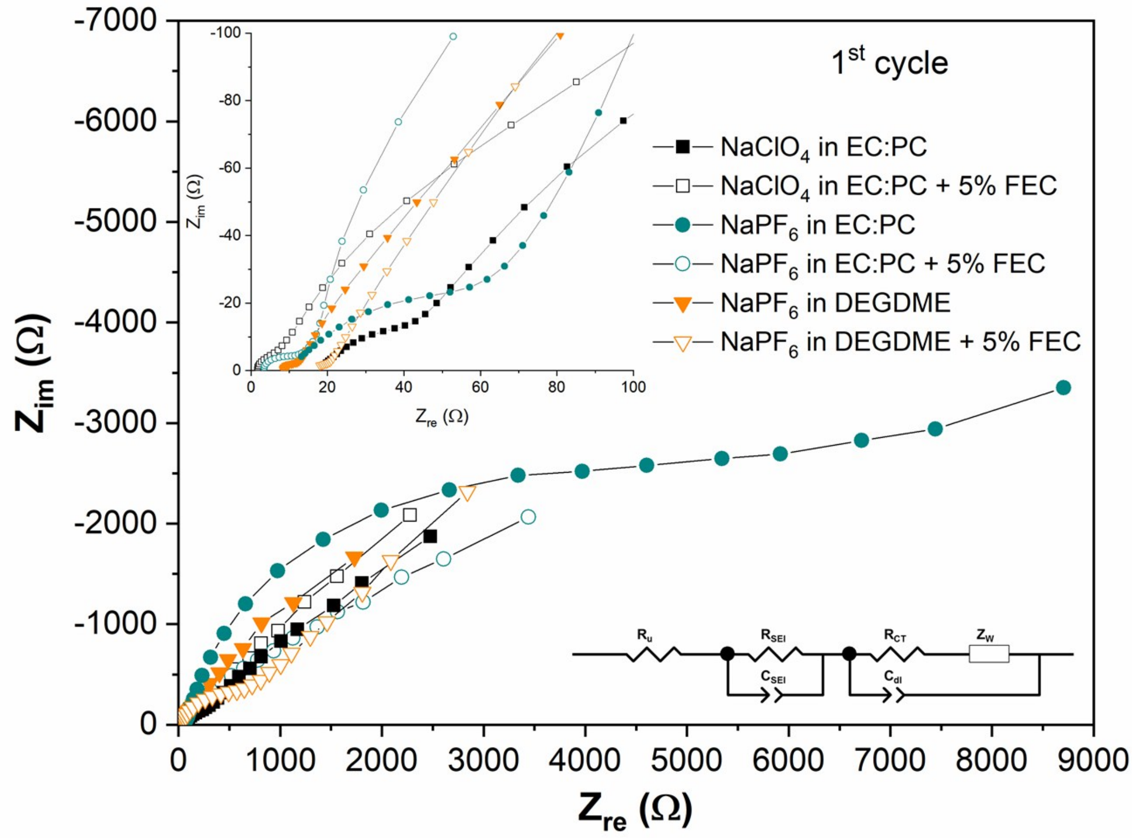

Figure S7. Electrochemical impedance spectroscopy of the Sn_4P_3/C electrodes cycled in the different electrolytes after the 1st cycle in the discharged (desodiated) state. The two insets show the equivalent circuit used for fitting the spectra and a zoom of the high frequency part.

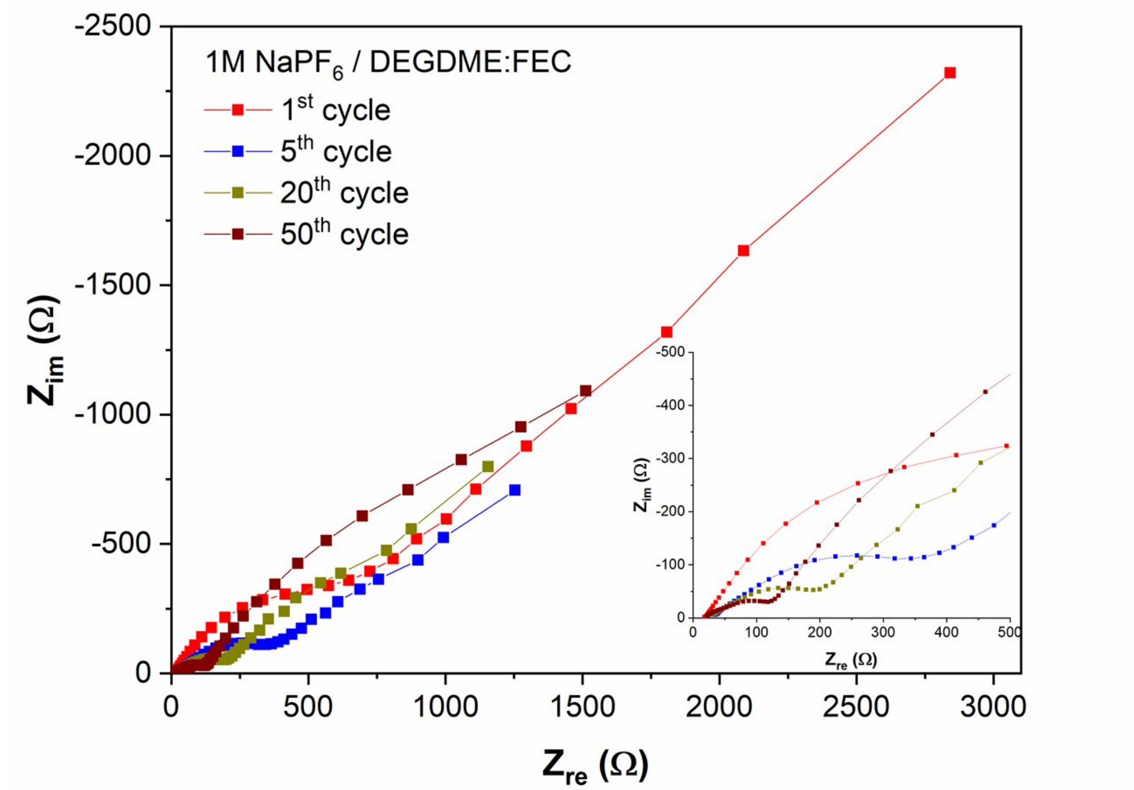

Figure S8. Electrochemical impedance spectroscopy of the Sn_4P_3/C electrodes cycled in $NaPF_6$/DEGDME:FEC electrolyte after the 1st, 5th, 20th and 50th in the discharged (desodiated) state. Inset shows a zoom of the high and middle frequency part.

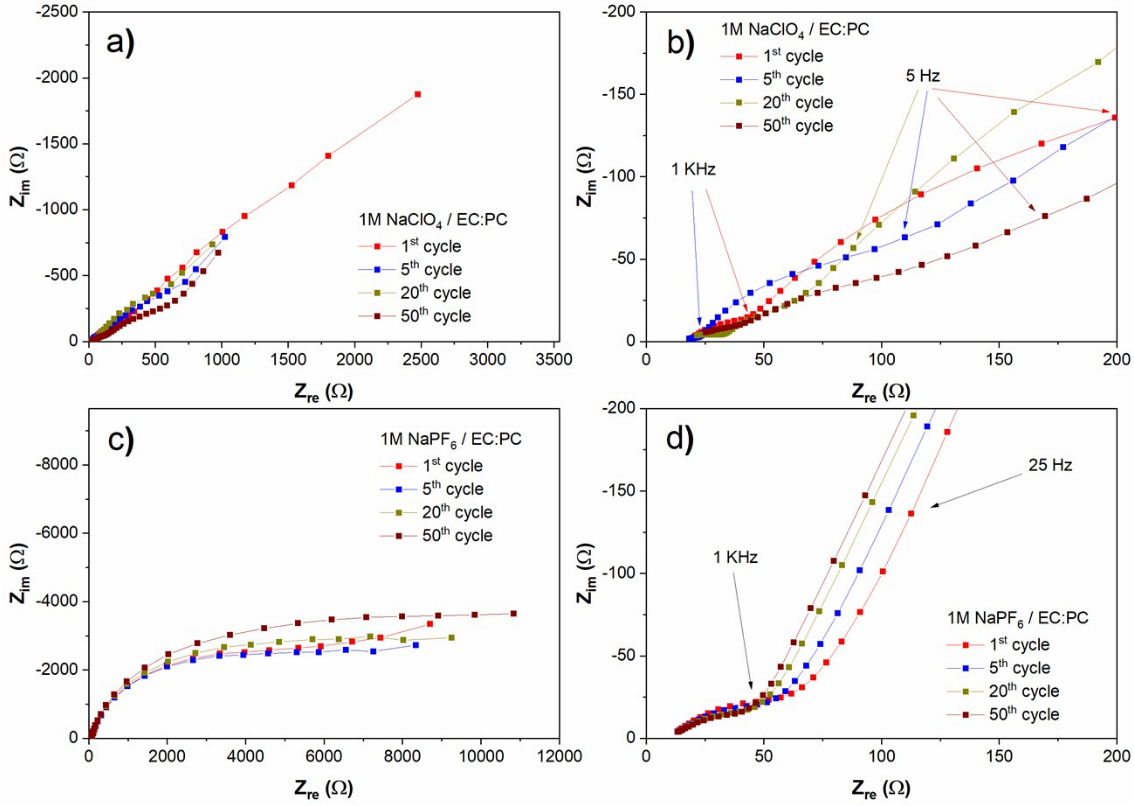

Figure S9. Electrochemical impedance spectroscopy of the Sn_4P_3/C electrodes cycled in $NaClO_4$/EC:PC (a, b) and $NaPF_6$/EC:PC (c, d) electrolytes after the 1st, 5th, 20th and 50th in the discharged (desodiated) state. Images b and d are zooms of the high and middle frequency part of figures a and c, respectively.

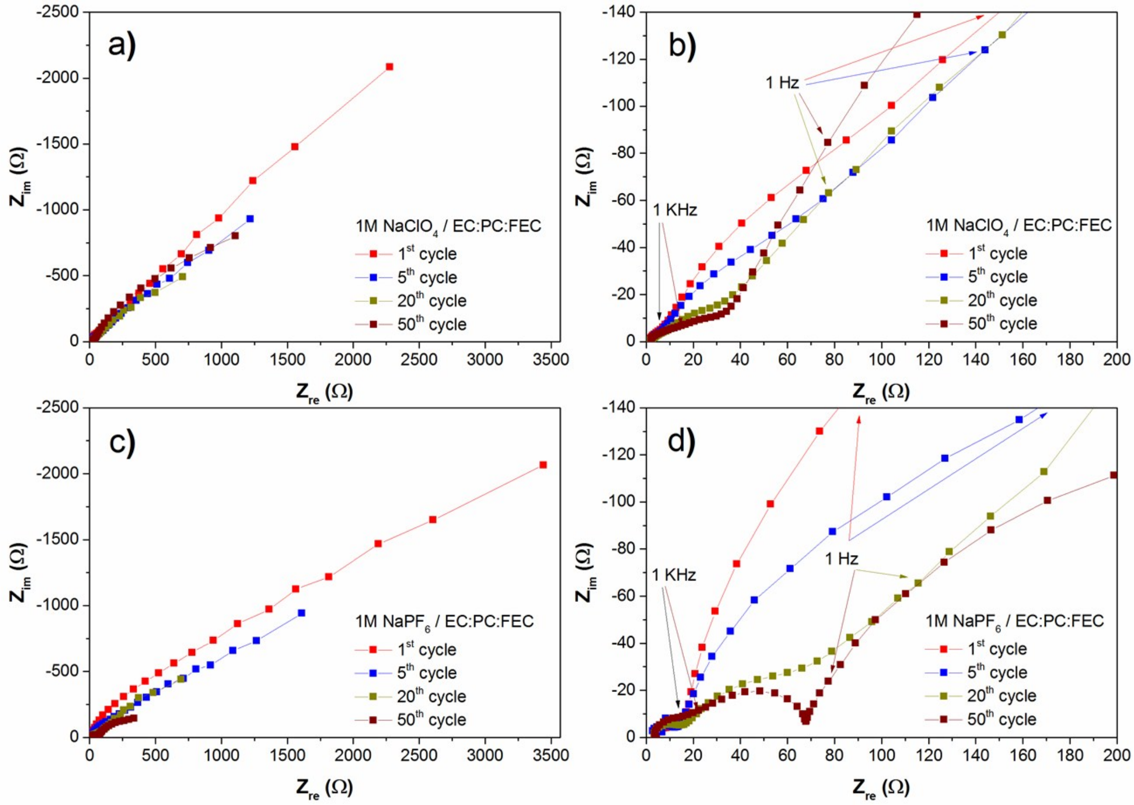

Figure S10. Electrochemical impedance spectroscopy of the Sn_4P_3/C electrodes cycled in $NaClO_4$/EC:PC:FEC (a, b) and $NaPF_6$/EC:PC:FEC (c, d) electrolytes after the 1st, 5th, 20th and 50th in the discharged (desodiated) state. Images b and d are zooms of the high and middle frequency part of figures a and c, respectively.

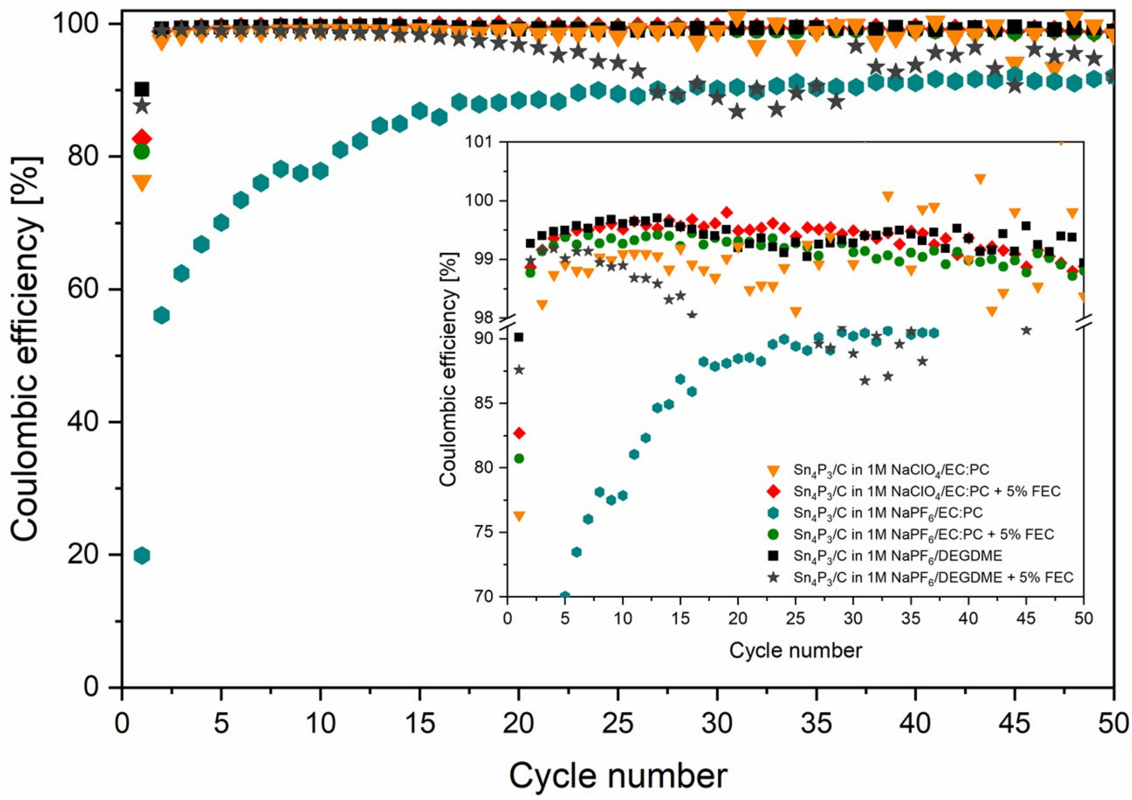

Figure S11. Coulombic efficiency of the Sn_4P_3@C electrodes cycled in $NaClO_4$/EC:PC:FEC, $NaPF_6$/EC:PC:FEC and $NaPF_6$/DEGDME electrolytes.

Table S1. Comparison of the electrochemical performance of our Sn_4P_3@C electrodes and the data obtained from the literature.

Synthesis method	**Material**	**Electrode formulation (active material/cond. add/binder) [%]**	**Electrolyte**	**Voltage window [V vs. Na^+/Na]**	**Reversible specific charge (current density) [mAh g^{-1} (mA g^{-1})]**	**Initial coulombic efficiency [%]**	**Capacity retention (%, nº cycles) [d]**	**Ref.**
High energy mechanical milling	Sn_4P_3	70/10/20 (a.m./Super P/PAA)	1M $NaClO_4$ in EC:DEC (1:1) + 5% FEC	1.5 – 0	833 (100) without FEC [a] 718 (100) with FEC [a]	~84% without FEC ~79% with FEC	~100%, 100 cy.	[1]
High energy mechanical milling	Sn_4P_3/C (70/30)	80/10/10 (a.m./Super P/CMC)	1M $NaPF_6$ in EC:DEC (1:1) + 5% FEC	2 – 0	816 (50) [a] 650 (100) [b] 560 (200) [b] 435 (500) [b] 349 (1000) [b]	77.3%	86%, 150 cy.	[2]
Low energy ball milling	$Sn_{4+x}P_3$@amorphous Sn-P	70/10/20 (a.m./carbon black/CMC)	1M $NaClO_4$ in EC:DEC (1:1) + 5% FEC	1.5 – 0	892 (100) [a] 543 (100) [b] 478.8 (200) [b] 423.3 (500) [b] 317.7 (1000) [b] 245.2 (2000) [b] 165.0 (5000) [b] 58.2 (10000) [b]	86.6%	72.1%, 100 cy.	[3]
Hydrothermal method	Yolk-shell Sn_4P_3@C (10% C)	70/20/10 (a.m./carbon black/PVDF)	1M $NaClO_4$ in PC + 5% FEC	2 – 0.01	711 (100) [a] 648 (200) [b] 586 (400) [b] 523 (800) [b] 455 (1500) [b] 379 (3000) [b]	43.8%	65.2%, 50 cy. @100 mA g^{-1} / 20%, 400 cy. @1500 mA g^{-1}	[4]
High energy mechanical milling	Sn_4P_3	70/10/20 (a.m./Super P/PAA)	1M $NaClO_4$ in EC:PC (1:1) / + FEC / + FEC +TMSP	1.5 – 0	1131 / 720 / 852 (C/20) [c]	~71% / 79.6% / 81.2%	30.3% / 76.9% / 92.3%, 50 cy. @C/10 [c]	[5]
Solvothermal method	Sn_4P_3	70/20/10 (a.m./carbon black/PVDF)	1M $NaClO_4$ in EC:DEC (1:1) + 5% FEC	3 – 0.01	647 (50)	52.8%	24.9%, 10 cy.	[6]

Solvothermal method	Sn_4P_3/rGO, 10.4% C	80/10/10 (a.m./carbon black/PVDF)	1M $NaClO_4$ in PC + 5% FEC	3 – 0.01	775 (100)	46.6%	84.6%, 100 cy.	[7]
Solvothermal method	Sn_4P_3	60/20/20 (a.m./Super P/CMC-PAA)	1M $NaClO_4$ in EC:PC (1:1) + 5% FEC	1.5 – 0.001	510 (100) 464 (5000)	59%	83%, 100 cy.	[8]
High energy mechanical milling	Sn_4P_3 / 0–30% TiC	80/10/10 (a.m./acetylene black/CMC)	1M $NaClO_4$ in PC + 5% FEC	1.5 – 0.01	532.3, 0%TiC (100) ~495, 10%TiC (100) ~420, 20%TiC (100) ~315, 30%TiC (100)	85.5% (0%TiC) 84.3% (10%TiC) 84.1% (20%TiC) 80.8% (30%TiC)	17.4%, 100 cy. (0% TiC) 41.1%, 100 cy. (10% TiC) 82.9%, 100 cy. (20% TiC) 94.5%, 100 cy. (30% TiC)	[9]
Purchased (Alfa-Aesar)	Commercial Sn_4P_3/MWCNT 20%	80/10/10 (a.m./carbon black/Na-alginate)	1M $NaClO_4$ in FEC/DMC (1:1)	1.5 – 0.01	520 – 501 (100) 500 (200) 464 (300) 397 (500) 259 (1000)	73.9%	90.2%, 120 cy.	[10]
Aerosol spray pyrolysis + thermal treatment	Sn_4P_3@C, 24% C	70/15/15 (a.m./carbon black/Na-alginate)	1M $NaPF_6$ in: 1) DME 2) EC:DMC (1:1) 3) EC:DMC (1:1) + 5% FEC	1.5 – 0	1) ~770 (100) 2) ~600 (100) 3) ~700 (100)	1) 90.7% @50 mA g^{-1} 2) 72.7% @50 mA g^{-1} 3) 59.8% @50 mA g^{-1}	1) 82%, 120 cy. @100 mA g^{-1} 2) 54%, 110 cy. @100 mA g^{-1} 3) 95%, 120 cy. @100 mA g^{-1}	[11]
Ball milling	Sn_4P_3/C, 12.5% C	80/10/10 (a.m./Super P/CMC)	1M $NaClO_4$ in PC + 5% FEC	2 – 0.01	~600 (100) ~510 (200) ~450 (500) ~385 (1000) ~255 (2000)	~82% @100 mA g^{-1}	~77%, 200 cy. @500 mA g^{-1} ~65%, 200 cy. @1000 mA g^{-1}	[12]
Solution chemistry method	Sn_4P_3	70/20/10 (a.m./MWCNT/CMC)	1M $NaClO_4$ in PC + 5% FEC	2 – 0	749 (50) 659 (100) 591 (200) 501 (500) 399 (1000)	72.7%	92%, 80 cy. @200 mA g^{-1} 82%, 50 cy. @500 mA g^{-1}	[13]
Hydrothermal method	Sn_4P_3-C, 19.4% C	70/20/10 (a.m./Super P/PAA)	1M $NaClO_4$ in EC:DMC + 5% FEC	2 – 0	721 (200) 680 (500) 495 (1000) 390 (2000) 260 (4000)	60%	90.1%, 50cy.	[14]

Solution chemistry + annealing + solvothermal	Sn4P3@C yolk-shell, n.d. %C	70/20/10 (a.m./acetylene black/PVDF)	1M $NaClO_4$ in PC + 5% FEC	2 – 0.01	771 (100) 725 (200) 642 (500) 583 (1000) 508 (2000)	63.7%	90.9%, 50 cy.	[15]
Ball milling	Sn_4P_3@C, 6% C	80/10/10 (a.m./Super C65/CMC)	1M $NaClO_4$ in EC:PC (1:1) + 5% FEC	1.5 – 0.005	507 (100) 432 (200) 340 (500) 270 (1000) 180 (2000) 80 (5000) 10 (10000)	82.7%	44.9%, 100 cy.	Our work
Ball milling	Sn_4P_3@C, 6% C	80/10/10 (a.m./Super C65/CMC)	1M $NaPF_6$ in EC:PC (1:1) + 5% FEC	1.5 – 0.005	505 (100) 432 (200) 345 (500) 270 (1000) 175 (2000) 85 (5000) 15 (10000)	80.7%	58.6%, 100 cy.	Our work
Ball milling	Sn_4P_3@C, 6% C	80/10/10 (a.m./Super C65/CMC)	1M $NaPF_6$ in DEGDME	1.5 – 0.005	820 (100) 740 (200) 660 (500) 570 (1000) 200 (2000) 170 (5000) 75 (10000)	90.1%	43.1%, 100 cy.	Our work

[a] 1st cycle reversible specific charge

[b] average specific charge at the given current density

[c] current density used to calculate C-rate was not specified

[d] Capacity retention at the lower current density, unless otherwise stated

References (Supporting information)

[1] Y. Kim, Y. Kim, A. Choi, S. Woo, D. Mok, N.-S. Choi, Y.S. Jung, J.H. Ryu, S.M. Oh, K.T. Lee, Tin Phosphide as a Promising Anode Material for Na-Ion Batteries, Adv. Mater. 26 (2014) 4139–4144. doi:10.1002/adma.201305638.

[2] J. Qian, Y. Xiong, Y. Cao, X. Ai, H. Yang, Synergistic Na-Storage Reactions in Sn_4P_3 as a High-Capacity, Cycle-stable Anode of Na-Ion Batteries, Nano Lett. 14 (2014) 1865–1869. doi:10.1021/nl404637q.

[3] W. Li, S.-L. Chou, J.-Z. Wang, J.H. Kim, H.-K. Liu, S.-X. Dou, $Sn_{4+x}P_3$ @ Amorphous Sn-P Composites as Anodes for Sodium-Ion Batteries with Low Cost, High Capacity, Long Life, and Superior Rate Capability, Adv. Mater. 26 (2014) 4037–4042. doi:10.1002/adma.201400794.

[4] J. Liu, P. Kopold, C. Wu, P.A. van Aken, J. Maier, Y. Yu, Uniform yolk–shell Sn_4P_3@C nanospheres as high-capacity and cycle-stable anode materials for sodium-ion batteries, Energy Env. Sci. 8 (2015) 3531–3538. doi:10.1039/C5EE02074C.

[5] J.Y. Jang, Y. Lee, Y. Kim, J. Lee, S.-M. Lee, K.T. Lee, N.-S. Choi, Interfacial architectures based on a binary additive combination for high-performance Sn_4P_3 anodes in sodium-ion batteries, J Mater Chem A. 3 (2015) 8332–8338. doi:10.1039/C5TA00724K.

[6] S. Liu, H. Zhang, L. Xu, L. Ma, X. Chen, Solvothermal preparation of tin phosphide as a long-life anode for advanced lithium and sodium ion batteries, J. Power Sources. 304 (2016) 346–353. doi:10.1016/j.jpowsour.2015.11.056.

[7] Q. Li, Z. Li, Z. Zhang, C. Li, J. Ma, C. Wang, X. Ge, S. Dong, L. Yin, Low-Temperature Solution-Based Phosphorization Reaction Route to Sn_4P_3/Reduced Graphene Oxide Nanohybrids as Anodes for Sodium Ion Batteries, Adv. Energy Mater. 6 (2016) 1600376. doi:10.1002/aenm.201600376.

[8] H.-S. Shin, K.-N. Jung, Y.N. Jo, M.-S. Park, H. Kim, J.-W. Lee, Tin phosphide-based anodes for sodium-ion batteries: synthesis via solvothermal transformation of Sn metal and phase-dependent Na storage performance, Sci. Rep. 6 (2016). doi:10.1038/srep26195.

[9] W. Wang, J. Zhang, D.Y.W. Yu, Q. Li, Improving the cycling stability of Sn 4 P 3 anode for sodium-ion battery, J. Power Sources. 364 (2017) 420–425. doi:10.1016/j.jpowsour.2017.08.060.

[10] J. Mao, X. Fan, C. Luo, C. Wang, Building Self-Healing Alloy Architecture for Stable Sodium-Ion Battery Anodes: A Case Study of Tin Anode Materials, ACS Appl. Mater. Interfaces. 8 (2016) 7147–7155. doi:10.1021/acsami.6b00641.

[11] X. Fan, T. Gao, C. Luo, F. Wang, J. Hu, C. Wang, Superior reversible tin phosphide-carbon spheres for sodium ion battery anode, Nano Energy. 38 (2017) 350–357. doi:10.1016/j.nanoen.2017.06.014.

[12] W. Zhang, J. Mao, W.K. Pang, Z. Guo, Z. Chen, Large-scale synthesis of ternary Sn 5 SbP 3 /C composite by ball milling for superior stable sodium-ion battery anode, Electrochimica Acta. 235 (2017) 107–113. doi:10.1016/j.electacta.2017.03.093.

[13] D. Lan, W. Wang, L. Shi, Y. Huang, L. Hu, Q. Li, Phase pure Sn_4P_3 nanotops by solution-liquid-solid growth for anode application in sodium ion batteries, J. Mater. Chem. A. 5 (2017) 5791–5796. doi:10.1039/C6TA10685D.

[14] J. Choi, W.-S. Kim, K.-H. Kim, S.-H. Hong, Sn_4P_3–C nanospheres as high capacitive and ultra-stable anodes for sodium ion and lithium ion batteries, J. Mater. Chem. A. (2018). doi:10.1039/C8TA05586F.

[15] L. Ma, P. Yan, S. Wu, G. Zhu, Y. Shen, Engineering tin phosphides@carbon yolk–shell nanocube structures as a highly stable anode material for sodium-ion batteries, J. Mater. Chem. A. 5 (2017) 16994–17000. doi:10.1039/C7TA04900E.